

Dual-Scale Nanostructures via Evaporative Assembly

Sunita Srivastava^{1*}, Zaibudeen A Wahith¹, Oleg Gang^{2,3,4}, Carlos E. Colosqui⁵, Surita R. Bhatia^{6*}

¹ Department of Physics, Indian Institute of Technology Bombay, Mumbai, India

²Center for Functional Nanomaterials, Brookhaven National Laboratory, Upton, NY, USA

³Department of Chemical Engineering, Columbia University, New York, NY, USA

⁴Department of Applied Physics and Applied Mathematics, Columbia University, New York, NY, USA

⁵Department of Mechanical Engineering, Stony Brook University, Stony Brook, NY, USA

⁶Department of Chemistry, Stony Brook University, Stony Brook, NY, USA

*Co-correponsing authors: sunita.srivastava@iitb.ac.in, surita.bhatia@stonybrook.edu

Abstract

Dual-scale hierarchical structures with regular microscale patterns and varying degree of nanoscale crystalline order are synthesized on physically and chemically homogeneous substrates by evaporative self-assembly with a suspension of DNA-functionalized nanoparticles (NPs) with a charged core shell. For a certain NP concentration range, periodic concentric rings in a stripe-like micropattern are produced over macroscale surface areas by a NP monolayer with hexagonal lattice structure at nanoscale. The stripe width, spacing and nanoparticle ordering can be controlled by varying the NP concentration. Our results indicate that the interplay between “stick-slip” motion of the droplet contact line and Coulombic and steric NP interactions control the formation of the observed structures. A simple analytical model is proposed to account for the experimental observations and guide the future design of different nanostructure morphologies. This work demonstrates a simple cost-effective mask-free method for fabricating large-area nanostructured 2D materials and metasurfaces for applications ranging from energy conversion/storage to optoelectronics and nanophotonics.

1. Introduction

The synthesis of nanoparticle (NP) films with ordered structures¹⁻⁷ in general and stripe patterns⁸⁻¹¹ in particular, has received substantial attention due to potential applications such as photonic crystal formation¹²⁻¹³, biochemical sensing¹⁴ surface plasmonics¹⁵⁻¹⁶, microelectronics¹⁷, or energy conversion and storage¹⁸. Surface patterning through bottom up self-assembly has emerged as a relatively simple and inexpensive technique for the fabrication of large-scale ordered structures on solid and soft substrates¹⁹⁻²². Solvent-evaporation based fabrication of long-range ordered surface patterns of nanoscale building blocks, provides an alternative to more complex methods such as mask-based lithography²³, Langmuir-Blodgett techniques²⁴⁻²⁵, dip-pen writing²⁶ and nanoimprinting;²⁷ and has been used for example to create free-standing nanoparticle superlattices.²⁸

The spontaneous pattern formation during evaporation of a sessile droplet of colloidal suspensions has been extensively studied since the first observations of the “coffee ring” effect that occurs due to deposition of solute particles around the three phase contact line (TCL)²⁹⁻³¹. The combination of outward flow driven by enhanced solvent evaporation at the droplet meniscus and the adhesion of solute particles to the substrate, results in the deposition of ring-like structures rich in solute particles at the TCL. Controlled evaporative assembly on plane substrates as well as systems with geometrical restrictions, has emerged as a novel method for creating patterned surfaces with diverse structures such as concentric rings^{6, 19, 32}, parallel lines/stripes^{8, 11, 33-34} and other patterns³⁵⁻³⁷. The formation of concentric rings has been attributed to the well-studied “stick-slip” motion of the TCL^{30, 38-41}. During this dual mode of evaporation, the TCL follows repetitive stick and slip stages of motion, which may result in either random or periodic pattern formation^{30, 36-39}. The stick-slip motion depends on several factors including the droplet size, substrate wettability, solute particle size and concentration.

These factors affect the microscale ordering and dimensions of resulting patterns (e.g., stripe/ring width and spacing).^{31, 42}

The formation of concentric ring or stripe-like patterns via stick-slip motion has been reported for dispersions of large NPs (>50 nm)^{34, 39}, patterned substrates,^{11, 35} polydispersed NPs (<25 nm)⁴⁻⁵, particle in polymer **solutions**^{37, 40, 43}, and in confined geometries.⁹⁻¹¹ Herein, we study the synthesis of dual-scale (i.e., micro/nanoscale) hierarchical 2D structures built by a NP monolayer deposited by evaporative assembly of DNA-functionalized gold NPs (DNA-NPs) of small diameter (15 nm). The studied system allows us to control NP repulsive interactions and thus the time scales for adhesion to the substrate, self-assembly, and crystallization. Multiscale hierarchically ordered structures are produced when such scales become comparable to those for stick-slip motion of the TCL. The morphologies obtained using the studied DNA-NPs at different concentrations range from disordered deposition, to continuous stripes of monolayers, to scalloped patterns; with different pseudo-crystalline structures at the nanoscale level. This study focuses on the conditions that lead to formation of regular concentric rings (i.e., stripe patterns), characterizing and predicting their structural morphology and evolution. The studied dual-scale structures are produced by a one-step evaporative-assembly process without chemical or physical templating and offers good tunability in ordering dimensions at different length scales, such as stripe width at microscale and lattice spacing at nanoscale.

We note that related reports of dual-scale patterning of particles either employ particles that are an order of magnitude or more larger than ours, or involve more complex processes for patterning. Pioneering work by Colvin⁴⁴ demonstrated patterning of colloidal crystals using larger 300 nm silica particles and repeated dip-coating of a vertical substrate. Ashurov *et al.*⁴⁵ reported formation of dual-scale stripe patterns of large 1.0 μm poly(styrene) colloids. Previous work by Watanabe *et al.*⁸ utilized 60-100 nm Au colloids, 120-270 nm silica colloids, and 200 nm poly(styrene) colloids; and relied on a convective assembly process employing a vertical

substrate with a liquid level that must be carefully controlled. Optical micrographs did show stripes in a system of 10-15 nm silver particles; however, these systems did not show a regular spacing between stripes nor nanoscale ordering of the particles within the stripes. This group has also reported grid patterns of 10-15 nm silver nanoparticles over a large area;⁴⁶ this is an impressive result but also utilized a two-step convective assembly process with a vertical substrate.

By contrast, our work focuses on nanometer-size particles and utilizes a single-step evaporative process on a horizontal substrate. We access a different regime of particles, leading to different physics than previous studies on micron and submicron particles. While hydrodynamic and capillary forces largely dominate the evaporative or convective assembly of microscale particles, short-range nanoscale interactions (e.g., steric and structural forces) and thermal motion play a crucial role in the self-assembly of nanoparticles. For the nanoparticles studied in our work, the timescales for self-assembly determined by such nanoscale interactions are comparable to the period for microscale stick-slip motion governed by hydrodynamic and capillary phenomena. This is a distinct and key aspect of the work. Understanding these phenomena on the nanoscale is crucial in order to apply evaporative assembly to applications involving nanoparticles; for example, for the assembly of quantum dots for bioanalysis, sensors, and **nanophotonics**.

2. Results and Discussion

This work documents and characterizes the formation of surface nanostructures with regular microscale patterns and nanoscale order produced from the evaporative deposition of DNA-NPs on hydrophilic silicon substrates described in detail in the Supporting Information. The employed DNA-NPs display negative zeta potentials (of the order of -10 mV) under the studied

neutral pH and concentration conditions and thus experience repulsive Coulombic interactions. Scanning Electron Microscopy (SEM) images in Fig. 1 show the deposited structures for DNA-NP suspensions in deionized (DI) water (Fig. 1a) and in 5 mM NaCl solution (Fig. 1b). In both cases the so-called “coffee-ring” effect is observed at the outer edge of the substrates where the droplet TCL is initially pinned. The formation mechanism for the observed “coffee-ring” has been extensively studied in previous works^{29, 41-42}. High magnification SEM images of the “coffee-ring” outer edge reveals multilayer nanoparticle deposition (Fig. S1, Supporting Information). The piranha-cleaned silicon substrate with DNA-NP suspensions display low contact angles, $\theta = 12 \pm 3$ deg for DI water and $\theta = 7 \pm 3$ deg for the NaCl salt solution in water. We acknowledge that it is difficult to accurately measure such low contact angles; however, we use the value of $\theta = 12$ deg as an estimate to obtain predictions from our analytical model, described below. The contact angle for DI water on the studied silicon substrates was found to be 41 ± 5 deg. These contact angle measurements (Fig. S2, Supporting Information) indicate that DNA-NP dispersed in the solvent at the studied concentrations produce the observed strong hydrophilic character of the substrates employed in our experiments.

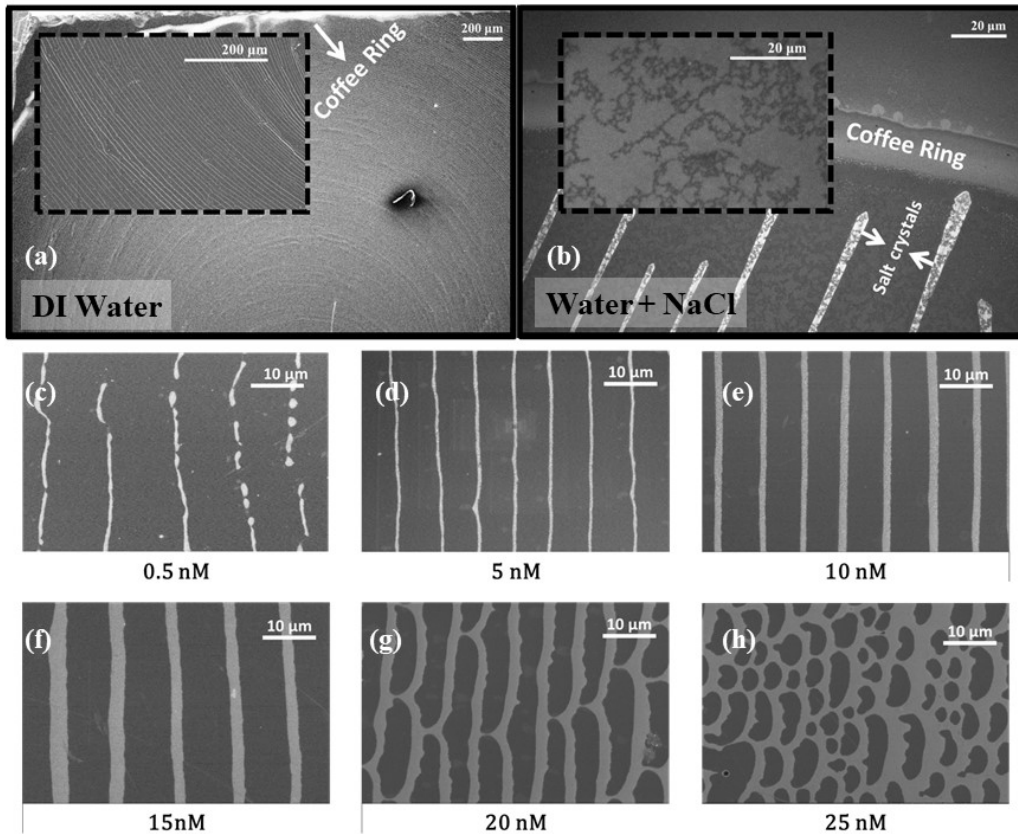


Figure 1. Microscale pattern morphologies (SEM images). (a) Deposited stripe-like pattern from DNA-NP suspension in DI water (NP concentration $c = 5$ nM). (b) Disordered deposition from DNA-NP suspension in 5 mM NaCl buffer solution ($c = 5$ nM). Insets of (a) and (b) at higher magnification have been reoriented. (c)-(h) Different microscale patterns produced with DNA-NP suspensions in DI water at indicated NP concentrations. Dotted and continuous stripe patterns (c-f) and scalloped patterns (g-h) are produced as shown.

The inner area of the evaporated droplet shows strikingly different structures for water and NaCl solutions. For surface samples produced by the evaporation of DNA-NP suspensions in DI water the outer “coffee-ring” deposit is followed by periodic concentric rings in the inner region of the substrate (Fig. 1a), whereas the DNA-NP dispersion in 5 mM NaCl solution results in the deposition of a disordered NP film underneath a layer of salt crystals (Fig. 1b). The presence of 5 mM NaCl in suspension effectively screens surface charges on the NPs and electrostatic repulsion becomes weak at distances larger than the Debye length ($\lambda_D \simeq 4$ nm), which results in the observed absence of periodic concentric rings (Fig. 1b). Our experimental observations thus indicate that long-range repulsive Coulombic interparticle interactions are required to produce the studied dual-scale nanostructures.

2.1. Dual-Scale Nanostructures by Evaporative Assembly

The microscale structure in the interior area of the evaporated droplets of DNA-NP suspensions in DI water exhibits complex morphological changes with the NP concentration c . Periodic microscale concentric rings resembling a stripe pattern are observed for concentrations $c \simeq 0.5$ to 15 nM (Figure 1c-g). On increasing the concentration beyond 15 nM, the observed microstructures evolve from striped to scalloped patterns (Figure 1g-h) having different length, depth, and surface area fraction covered by NPs.

The main focus of this work is to study the self-assembled surface structures within the NP concentration range ($0.5 \text{ nM} < c \leq 15 \text{ nM}$) that leads to the formation of concentric periodic rings of microscale dimensions in a stripe pattern. As shown in Fig. 2 for the case of NPs of 15 nm diameter, high magnification SEM images reveal NP ordering at micro- and nanoscale levels and, hence, the formation of dual-scale hierarchically ordered 2D structures. The multiple concentric NP rings observed at macroscale level (Fig. 2a) form a stripe pattern at microscale level (Fig. 2b) with the deposited stripes composed of a hexagonally ordered NP monolayer at nanoscale level (Fig. 2c).

It is worth noticing that a gradual variation of the width and spacing of the assembled stripe pattern can be measured over lengths of several hundred microns as one moves toward the center of the substrate. This morphology variation is expected given that changes in the droplet contact radius and contact angle are known to affect the time scales of the stick-slip motion⁴⁷⁻⁴⁹. However, at a fixed distance from the outer edge of the substrate, the stripe width and spacing consistently show the reported dependence on NP concentration that is analyzed in the following section.

An additional item of note is that the stripe edge corresponding to the outer side of the receding droplet (the left edge in Figs. 2 and 3) tends to be more uniform than the opposite edge. This suggests that after slip occurs, the TCL leads to a somewhat straighter edge as compared to the

inner edge. We expect this may occur because the leading edge of the deposits can relax over longer times under the “pull” of the receding of the contact line. However, the SEM images themselves do not provide sufficient evidence for this mechanism; we will explore it further in future studies.

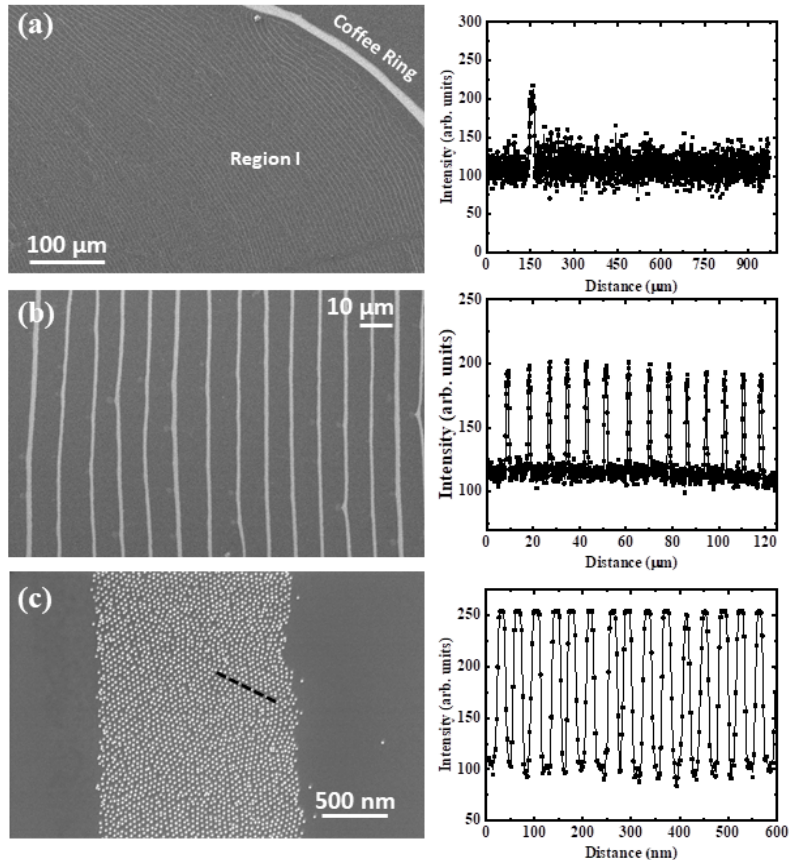


Figure 2. Dual-scale surface nanostructure morphology for a deposited DNA-NP suspension in DI water ($c = 10$ nM, NP diameter 15 nm). Figures are oriented such that the TCL moves from left to right. (a) Macroscale level observation of the “coffee-ring” effect (i.e., multilayer NP outer ring assembly) and periodic concentric rings in a stripe-like pattern within the enclosed inner surface (Region I). (b) Microscale level stripe pattern with uniform stripe w width and distance d . (c) Nanoscale level observation of a NP monolayer organized into a hexagonal close-packed 2D lattice (the dashed line in SEM image indicates the scanned direction for intensity profile).

2.2 Morphology Dependence on Nanoparticle Concentration

Here, we will focus on the analysis of the width and spacing of periodic concentric rings (i.e., stripe patterns) observed for the NP concentration range 0.5 to 15 nM (Fig. 3). The observed microscale stripes typically extend over a substrate area measuring several square millimeters

(SEM image Fig. 1a). The stripes align parallel to the receding TCL, which is consistent with so-called “stick-slip” motion reported in previous literature^{6, 19, 30, 39-40}. Furthermore, high magnification SEM images reveal that the deposited stripes are made of a crystalline NP monolayer (cf. Fig. 3e-f); the degree of ordering is confirmed by the radial Fourier transform of the SEM images within the stripes (Fig. 3i-l). Additional images are provided in the Supporting Information.

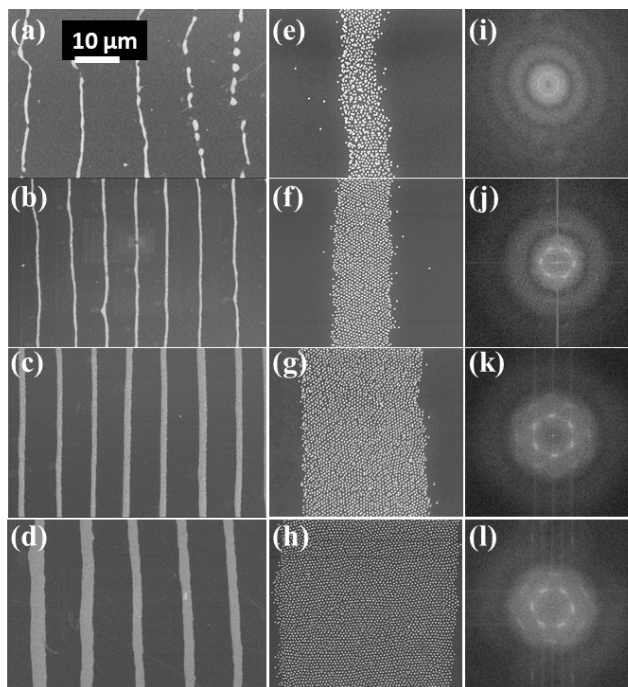


Figure 3: Dual-scale hierarchical order for different DNA-NP concentration. Figures are oriented such that the TCL moves from left to right. (a)-(d) SEM images showing microscale stripe patterns and nanoscale NP monolayer structure inside the deposited stripes at 0.5 nM, 5 nM, 10 nM and 15 nM respectively. Above a critical concentration (~ 5 nM) the deposited NP monolayer forms continuous stripes as shown in (b). (e)-(h) Increased magnification of the deposited stripes corresponding to samples in (a)-(d), respectively. (i)-(l) Radial Fourier transform of the SEM image within the deposited stripes, demonstrating that the NP monolayer structure transitions from loosely packed to highly ordered hexagonal lattices for $c \geq 5$ nM.

For low NP concentrations ($c \leq 5$ nM), we observe broken irregular stripes composed of amorphous NP assemblies (see inset in Fig. 3a at $c = 0.5$ nM). For larger NP concentrations ($c = 5$ to 15 nM), regular stripes are composed by nearly crystalline assemblies (see inset in Fig. 3b) with a uniform spacing $s = 34 \pm 3$ nm. Fourier analysis of the SEM images (Fig. 3g) confirms the assembly of nanoparticle in a hexagonal lattice within the stripes formed for $c \geq 5$ nM. The degree of local ordering at nanoscale level varies with the NP concentration. At low

concentration the hexagonal NP assembly is accompanied with minor defects, and evolves into well-ordered hexagonal lattice with an increase in concentration. The NP crystallization and spacing within the deposited microscale stripes is controlled by repulsive Coulombic and steric interactions due to the negatively charged DNA chains grafted on the NP surface.

2.3. Analytical Model for the Stripe Morphology

For the concentration range $0.5 < c \leq 15$ nM and the substrate region where the deposited NP concentric stripes have a radius $R \simeq 1$ mm, the measured the distance between stripes varies from 6 to 12 μm (Figure 4a) and the stripe width varies between 0.5 and 3 μm (Figure 4b). For sufficiently large concentrations $c \geq 5$ nM for which the formed stripes are continuous and regular, the distance between stripes ($d \simeq 6 \mu\text{m}$) depends weakly on the concentration and the stripe width increases linearly with concentration. A simple model to account for these observations and make quantitative predictions for the stripe pattern morphology is obtained by considering that the TCL undergoes periodic “stick-slip” motion (Fig. 4c-e) as a droplet of the NP suspension evaporates. In accordance with our experimental observations, the model assumes that only monolayers are formed. We expect that we do not observe multilayers due to the hydrophilicity of the surface (i.e., very low receding contact angles) and the low volume fractions employed in our experiments. We also note that Watanabe *et al.* have previously proposed a model for convective assembly of larger particles⁵⁰ that accounts for the impact of a concavely curved meniscus. This mechanism is not able to account for the variation of stripe width and spacing of the monolayer stripes observed in our experiments. It is probable that the mechanism suggested by Watanabe *et al.* dominates the dynamics and morphology for the case of multilayerd deposits and/or larger particles for which surface energy minimization and associated capillary effects become largely dominant.

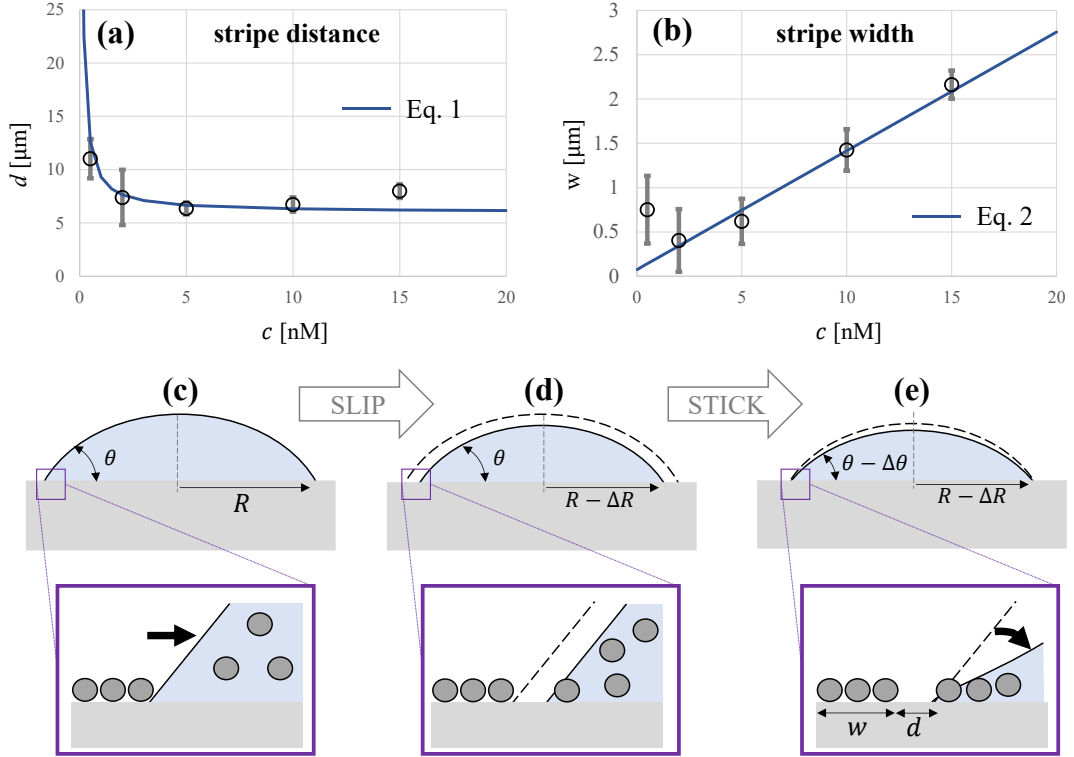


Figure 4: Stripe pattern morphology and formation mechanism. (a) Stripe distance vs. molar concentration. (b) Stripe width vs. molar concentration. Markers indicate experimental results (NP diameter 15 nm). Solid lines are analytical fits via Equation 1 and 2 for TCL radius $R = 1$ mm, receding contact angle $\theta = 12$ deg, lattice spacing $s = 34$ nm, minimum stripe distance $d_o = 6$ μm , NP adsorption energy $E_a = 0.7 k_B T$, and 15-nm NP diameter. (c-e) Illustration of the droplet and TCL configuration during stick-slip motion at: (c) the start of the slip stage; (d) end of the slip stage (i.e., full TCL pinning); (e) the stick stage. Analytical predictions are based (see text) on the illustrated mechanism and TCL relaxation process with $\cos \theta \approx 1$ and $\Delta R \ll R$.

Immediately after detaching from a deposited NP assembly the droplet contact radius R decreases and the contact angle θ remains constant (Fig. 4c) over a finite slip time τ_s , during which negligible number of NPs are able to reach the TCL and adsorb to the surface. The slip time τ_s is determined by dynamic effects, the particle concentration, and the adsorption free energy E_a , and prescribes the minimum distance d_o observed between stripes. We further assume that a critical number of particles N_p must be transported to the TCL and adsorbed so that the full contact line stops receding (Fig. 4d) and further droplet evaporation becomes mediated by a decrease in the contact angle (Fig. 4e) as the contact radius remains constant.

There is a minimum number of adsorbed particles $N_p \simeq f_w/f_p$ that can fully stop a receding liquid-vapor interface⁵¹⁻⁵², which for the case of highly hydrophilic substrate and particles is determined by the wetting force magnitude $f_w = 2\pi\gamma R$ acting on the contact line and the pinning force of a single particle $f_p = 2\pi\gamma R_p \sin\theta$; here, γ is the water-vapor surface tension and R_p is the particle radius. During the slip stage of “stick-slip” motion (Fig. 4c) the droplet is assumed to evaporate at a constant volumetric rate $\dot{V} = 3\pi R^2 f_V(\theta) \times dR/dt$, where $f_V(\theta) = [(2/3) - (3/4)\cos\theta + (1/12)\cos3\theta]/\sin3\theta$ is the shape function for a spherical cap. Hence, when the TCL recedes a small distance $\Delta R \ll R$ a number of particles $N_s \simeq 3\pi R^2 \Delta R f_V(\theta) \times c N_A$ (here, N_A is Avogadro’s number) are transported to the wedge region near the droplet TCL²⁹. Accordingly, the TCL must become pinned after receding a distance

$$d = d_o + \frac{N_p}{3\pi R^2 f_V(\theta)} \times \frac{1}{c N_A}, \quad (1)$$

which in turn determines the observed spacing between stripes (Fig. 4a). For the studied experimental conditions, we observe that $d \simeq d_o \simeq 6 \mu\text{m}$ for $5 \leq c \leq 10 \text{ nM}$ (Fig. 4a), and the slip time τ_s seems to weakly depend on the NP concentration within that range.

After the TCL is pinned by the adsorbed NPs (Fig. 4c-d), the contact angle decreases substantially, which prevents further transport of NPs to the TCL. The number of particles $N_s(d) \simeq d \times 3\pi R^2 f_V(\theta) \times c N_A \geq N_p$ transported to the contact line wedge in the slip stage, continue to adsorb and assemble under near-equilibrium conditions during the stick stage when the TCL is pinned at a nearly static position where a new stripe is formed. The number of particles adsorbed $N_a = N_s(d) \exp(-E_a/k_B T)$ on the surface under near-equilibrium conditions during the stick stage is prescribed by the adsorption free energy $E_a \sim k_B T$ (here, $k_B T$ is the thermal energy). For sufficiently long pinning times, determined by the wetting conditions, droplet and particle size, the studied DNA-NPs can assemble in a hexagonal lattice

with constant spacing s , which results in surface area density $\phi_A = 2/(\sqrt{3}s^2)$. We can thus estimate the stripe width

$$w = d \times \frac{3Rf_V(\theta)}{2\phi_A} \times cNA \times \exp(-E_a/k_B T) \quad (2)$$

from the stripe spacing d given by Equation 1.

The observed stripe spacing and width (Fig. 4a-b) can be fitted by analytical predictions from Equation 1 and 2 by employing the experimentally determined contact angle $\theta = 12$ deg, NP lattice spacing $s = 34$ nm, and minimum stripe distance $d_o \simeq 6$ μm , assuming a droplet contact radius $R = 1$ mm and adsorption energy $E_a = 0.7 k_B T$. While the contact radius of 1 mm corresponds to that observed in the reported experiments, the adsorption energy of $0.7 k_B T$ is obtained by fitting the experimental data in Fig. 4b. The stripe distance (Fig. 4a) shows a slight increase with concentration for $c > 10$ nM, which can be attributed to a weak increase of the slip time τ_s with the NP concentration that indicates the transition from regular stripes to complex scalloped patterns observed at $c > 15$ nM (Fig. 1g-h). At low concentrations $c \leq 5$ nM, for which the formed stripes are not continuous and the average NP spacing increases, the measured width (Fig. 4b) is higher than predicted by Equation 1, which considers a hexagonal NP lattice with constant spacing.

3. Conclusion

We have demonstrated the synthesis over large (cm^2) areas of dual-scale (i.e., micro/nanoscale) hierachal surface structures comprising a monolayer of DNA-functionalized (15-nm) gold NPs by a simple and cost-effective evaporative self-assembly method. The microscale morphology exhibits good tunability with NP concentration and gradual structural transitions from dotted and continuous stripes to scalloped patterns. On increasing the NP concentration, the nanoscale

structure transitions from loosely packed to highly ordered hexagonal lattices. Above a critical concentration (~ 5 nM) the deposited NP monolayer self-assembles into a hexagonal lattice with uniform spacing prescribed by Coloumbic and steric interactions that can be tuned via NP functionalization. An analytical model is proposed to account for experimental observations by considering stick-slip motion due to TCL self-pinning and a finite NP adsorption energy ($E_A \sim k_B T$). The derived analytical predictions can be employed to guide the fabrication and design of nanostructured materials and metasurfaces where it is essential to control the period and regularity of their micro- and nanoscale structures.

4. Experimental Section

Nanoparticle functionalization and dispersion: The gold NPs were purchased from Ted Pella and their mean sizes as measured by small angle x-ray scattering are 15 nm. The nanoparticles were functionalized with non-complementary single stranded thiolated DNA chains (Integrated DNA technologies) using the protocol described elsewhere in detail. The sequence details of the DNA chains used is given in the Supplementary Information (Table 1). Briefly, the thiolated DNA was reduced using high concentration of DTT, the reduced DNA was added to the nanoparticle solution in ratio of 100X for spherical particles. After few hours of incubation, the salting process was done using stock solution of 3 M NaCl followed by cleaning and re-dispersion in water. The cleaning process was repeated multiple times to ensure no residue of salt in the final dispersion. The concentration of the DNA functionalized nanoparticles was determined using a UV-vis absorption spectroscopy (Figure S1). DNA-NP suspensions of concentration ~ 0.5 – 25 nM were prepared. Ultrapure water (Millipore, 18.2 MU-cm) was used throughout sample preparation. All other chemicals used in this study were purchased from Sigma Aldrich. After functionalization, the measured zeta potential of the

suspended NPs in water was negative (on the order of -10mV at neutral pH and the concentrations studied), which indicates repulsive interparticle interactions.

Droplet deposition and evaporation: Single-sided polished silicon wafers with $<100>$ orientation and a native oxide layer were employed as substrates after a thorough cleaning process. The silicon wafers were washed with acetone (99.9%, Sigma Aldrich), ethanol and ultrasonicated in deionized water bath for few seconds as a preliminary cleaning procedure. After initial cleaning, the substrates were treated with Piranha solution (3:1 mixture of H_2SO_4 and H_2O_2) for 15 min at 70°C followed by washing with DI water. This process removes contamination and oxides from the surface and renders the silicon substrates hydrophilic. Immediately, before drop casting the DNA-NP solution, the substrates were blow-dried under a high-pressure stream of nitrogen gas. Once air-dried the substrates were immediately used for drop casting of the DNA-NP dispersion. Typically, 1 to 2 μL of solution were used for drop casting on the freshly cleaned substrate ($0.5 \times 0.5 \text{ cm}^2$) and the system was left undisturbed in a clean environment. The DNA-NP solution spreads spontaneously to form a drop of low contact angle ~ 12 deg that indicates a strong hydrophilic character of the silicon substrate. Typically it takes $\sim 8\text{-}10$ mins for the droplet to evaporate, however a drying time of ~ 12 hours was employed before SEM characterization. The contact angle and optical measurements were done in-situ under the same experimental conditions. The above evaporation process results in self-assembly over a relatively large area ($\sim \text{cm}^2$). Every experiment was repeated several times in order to establish reproducibility.

Supporting Information

Supporting Information is available from the Wiley Online Library or from the author.

Acknowledgements

This work was supported by the National Science Foundation, Award No. CBET-1335787 and CBET-1903189. CEC acknowledges support from ONR Award N00014-16-1-3178. This research used resources of the Center for Functional Nanomaterials, which is a U.S. DOE Office of Science Facility, at Brookhaven National Laboratory under Contract No. DE-SC0012704.

Received: ((will be filled in by the editorial staff))

Revised: ((will be filled in by the editorial staff))

Published online: ((will be filled in by the editorial staff))

References

1. Bigioni, T. P.; Lin, X. M.; Nguyen, T. T.; Corwin, E. I.; Witten, T. A.; Jaeger, H. M., Kinetically driven self assembly of highly ordered nanoparticle monolayers. *Nature Materials* **2006**, *5* (4), 265-270.
2. Srivastava, S.; Nykypanchuk, D.; Fukuto, M.; Halverson, J. D.; Tkachenko, A. V.; Yager, K. G.; Gang, O., Two-Dimensional DNA-Programmable Assembly of Nanoparticles at Liquid Interfaces. *Journal of the American Chemical Society* **2014**, *136* (23), 8323-8332.
3. Ming, T.; Kou, X. S.; Chen, H. J.; Wang, T.; Tam, H. L.; Cheah, K. W.; Chen, J. Y.; Wang, J. F., Ordered Gold Nanostructure Assemblies Formed By Droplet Evaporation. *Angewandte Chemie-International Edition* **2008**, *47* (50), 9685-9690.
4. Lerond, T.; Proust, J.; Yockell-Lelievre, H.; Gerard, D.; Plain, J., Self-assembly of metallic nanoparticles into plasmonic rings. *Applied Physics Letters* **2011**, *99* (12).
5. Chen, J. X.; Liao, W. S.; Chen, X.; Yang, T. L.; Wark, S. E.; Son, D. H.; Batteas, J. D.; Cremer, P. S., Evaporation-Induced Assembly of Quantum Dots into Nanorings. *Acs Nano* **2009**, *3* (1), 173-180.
6. Zhang, S. F.; Luan, W. L.; Zhong, Q. X.; Yin, S. F.; Yang, F. Q., Evaporation-induced self-assembly of quantum dots-based concentric rings on polymer-based nanocomposite films. *Soft Matter* **2016**, *12* (40), 8285-8296.
7. Talapin, D. V.; Shevchenko, E. V., Introduction: nanoparticle chemistry. ACS Publications: 2016.
8. Watanabe, S.; Mino, Y.; Ichikawa, Y.; Miyahara, M. T., Spontaneous Formation of Cluster Array of Gold Particles by Convective Self-Assembly. *Langmuir* **2012**, *28* (36), 12982-12988.
9. Li, B.; Zhang, C. C.; Jiang, B. B.; Han, W.; Lin, Z. Q., Flow-Enabled Self-Assembly of Large-Scale Aligned Nanowires. *Angewandte Chemie-International Edition* **2015**, *54* (14), 4250-4254.
10. Sun, Y. J.; Lin, Y.; Su, Z. H.; Wang, Q., One-step assembly of multi-layered structures with orthogonally oriented stripe-like patterns on the surface of a capillary tube. *Physical Chemistry Chemical Physics* **2017**, *19* (35), 23719-23722.
11. Li, X. M.; Wang, C. H.; Shao, J. Y.; Ding, Y. C.; Tian, H. M.; Li, X. M.; Wang, L., Periodic Parallel Array of Nanopillars and Nanoholes Resulting from Colloidal Stripes Patterned by Geometrically Confined Evaporative Self-Assembly for Unique Anisotropic Wetting. *Acs Applied Materials & Interfaces* **2014**, *6* (22), 20300-20308.
12. Joannopoulos, J. D.; Villeneuve, P. R.; Fan, S. H., Photonic crystals: Putting a new twist on light. *Nature* **1997**, *386* (6621), 143-149.
13. Kim, H.; Ge, J. P.; Kim, J.; Choi, S.; Lee, H.; Lee, H.; Park, W.; Yin, Y.; Kwon, S., Structural colour printing using a magnetically tunable and lithographically fixable photonic crystal. *Nature Photonics* **2009**, *3* (9), 534-540.

14. Lu, Y.; Liu, G. L.; Kim, J.; Mejia, Y. X.; Lee, L. P., Nanophotonic crescent moon structures with sharp edge for ultrasensitive biomolecular detection by local electromagnetic field enhancement effect. *Nano Letters* **2005**, 5 (1), 119-124.

15. Ye, J.; Wen, F. F.; Sobhani, H.; Lassiter, J. B.; Van Dorpe, P.; Nordlander, P.; Halas, N. J., Plasmonic Nanoclusters: Near Field Properties of the Fano Resonance Interrogated with SERS. *Nano Letters* **2012**, 12 (3), 1660-1667.

16. Lal, S.; Link, S.; Halas, N. J., Nano-optics from sensing to waveguiding. *Nature Photonics* **2007**, 1 (11), 641-648.

17. Jacobs, H. O.; Whitesides, G. M., Submicrometer patterning of charge in thin-film electrets. *Science* **2001**, 291 (5509), 1763-1766.

18. Zhang, Q.; Uchaker, E.; Candelaria, S. L.; Cao, G., Nanomaterials for energy conversion and storage. *Chemical Society Reviews* **2013**, 42 (7), 3127-3171.

19. Zhang, L.; Maheshwari, S.; Chang, H. C.; Zhu, Y. X., Evaporative self-assembly from complex DNA-colloid suspensions. *Langmuir* **2008**, 24 (8), 3911-3917.

20. Srivastava, S.; Nykypanchuk, D.; Fukuto, M.; Gang, O., Tunable Nanoparticle Arrays at Charged Interfaces. *Acs Nano* **2014**, 8 (10), 9857-9866.

21. Byun, M.; Hong, S. W.; Zhu, L.; Lin, Z. Q., Self-assembling semicrystalline polymer into highly ordered, microscopic concentric rings by evaporation. *Langmuir* **2008**, 24 (7), 3525-3531.

22. Wu, L. L.; Wang, X.; Wang, G.; Chen, G., In situ X-ray scattering observation of two-dimensional interfacial colloidal crystallization. *Nature Communications* **2018**, 9.

23. Xiao, J. Y.; Li, Z.; Ye, X. Z.; Ma, Y. R.; Qi, L. M., Self-assembly of gold nanorods into vertically aligned, rectangular microplates with a supercrystalline structure. *Nanoscale* **2014**, 6 (2), 996-1004.

24. Huang, C. Y.; Lu, N.; Chi, L. F., Surface patterning approaches based on Langmuir-Blodgett technique. *Progress in Chemistry* **2007**, 19 (6), 852-859.

25. Zhou, X. Q.; Cao, H.; Yang, D.; Zhang, L.; Jiang, L.; Liu, M. H., Two-Dimensional Alignment of Self-Assembled Organic Nanotubes through Langmuir-Blodgett Technique. *Langmuir* **2016**, 32 (49), 13065-13072.

26. Lim, J. H.; Mirkin, C. A., Electrostatically driven dip-pen nanolithography of conducting polymers. *Advanced Materials* **2002**, 14 (20), 1474-+.

27. de Gans, B. J.; Schubert, U. S., Inkjet printing of well-defined polymer dots and arrays. *Langmuir* **2004**, 20 (18), 7789-7793.

28. Cheng, W.; Campolongo, M. J.; Cha, J. J.; Tan, S. J.; Umbach, C. C.; Muller, D. A.; Luo, D., Free-standing nanoparticle superlattice sheets controlled by DNA. *Nature materials* **2009**, 8 (6), 519.

29. Deegan, R. D.; Bakajin, O.; Dupont, T. F.; Huber, G.; Nagel, S. R.; Witten, T. A., Capillary flow as the cause of ring stains from dried liquid drops. *Nature* **1997**, 389 (6653), 827-829.

30. Adachi, E.; Dimitrov, A. S.; Nagayama, K., Stripe Patterns Formed on a Glass-Surface during Droplet Evaporation. *Langmuir* **1995**, 11 (4), 1057-1060.

31. Mampallil, D.; Eral, H. B., A review on suppression and utilization of the coffee-ring effect. *Advances in Colloid and Interface Science* **2018**, 252, 38-54.

32. Bi, W. G.; Wu, X. Y.; Yeow, E. K. L., Unconventional Multiple Ring Structure Formation from Evaporation-Induced Self-Assembly of Polymers. *Langmuir* **2012**, 28 (30), 11056-11063.

33. Li, H.; Hain, T. C.; Muzha, A.; Schoppler, F.; Hertel, T., Dynamical Contact Line Pinning and Zipping during Carbon Nanotube Coffee Stain Formation. *Acs Nano* **2014**, 8 (6), 6417-6424.

34. Lin, Y.; Balizan, E.; Lee, L. A.; Niu, Z. W.; Wang, Q., Self-Assembly of Rodlike Bio-nanoparticles in Capillary Tubes. *Angewandte Chemie-International Edition* **2010**, 49 (5), 868-872.

35. Zhou, H. H.; Huang, Z. D.; Cai, Z. R.; Zhang, R.; Wang, H. Y.; Song, Y. L.; Reichmanis, E., Patterning Bubbles by the Stick-Slip Motion of the Advancing Triple Phase Line on Nanostructures. *Langmuir* **2018**, 34 (51), 15804-15811.

36. Takhistov, P.; Chang, H. C., Complex stain morphologies. *Industrial & Engineering Chemistry Research* **2002**, 41 (25), 6256-6269.

37. Ryu, S. A.; Kim, J. Y.; Kim, S. Y.; Weon, B. M., Drying-mediated patterns in colloid-polymer suspensions. *Scientific Reports* **2017**, 7.

38. Deegan, R. D., Pattern formation in drying drops. *Physical Review E* **2000**, *61* (1), 475-485.

39. Shmuylovich, L.; Shen, A. Q.; Stone, H. A., Surface morphology of drying latex films: Multiple ring formation. *Langmuir* **2002**, *18* (9), 3441-3445.

40. Maheshwari, S.; Zhang, L.; Zhu, Y. X.; Chang, H. C., Coupling between precipitation and contact-line dynamics: Multiring stains and stick-slip motion. *Physical Review Letters* **2008**, *100* (4).

41. Denkov, N. D.; Velev, O. D.; Kralchevsky, P. A.; Ivanov, I. B.; Yoshimura, H.; Nagayama, K., Mechanism of Formation of 2-Dimensional Crystals from Latex-Particles on Substrates. *Langmuir* **1992**, *8* (12), 3183-3190.

42. Patil, N. D.; Bhardwaj, R., Recent Developments on Colloidal Deposits Obtained by Evaporation of Sessile Droplets on a Solid Surface. *Journal of the Indian Institute of Science* **2019**, *99* (1), 143-156.

43. Zhang, C. F.; Akcora, P., Evaporation controlled particle patterns in a polymer droplet. *Rsc Advances* **2017**, *7* (30), 18321-18326.

44. Jiang, P.; Bertone, J.; Hwang, K. S.; Colvin, V., Single-crystal colloidal multilayers of controlled thickness. *Chemistry of Materials* **1999**, *11* (8), 2132-2140.

45. Ashurov, M.; Eremina, E.; Laptinskaya, T.; Klimonsky, S., Self-assembly of polystyrene microspheres into two-level hierarchical structures. *Superlattices and Microstructures* **2018**, *120*, 806-811.

46. Mino, Y.; Watanabe, S.; Miyahara, M. T., Colloidal stripe pattern with controlled periodicity by convective self-assembly with liquid-level manipulation. *ACS applied materials & interfaces* **2012**, *4* (6), 3184-3190.

47. Moffat, J. R.; Sefiane, K.; Shanahan, M. E., Effect of TiO₂ nanoparticles on contact line stick-slip behavior of volatile drops. *The Journal of Physical Chemistry B* **2009**, *113* (26), 8860-8866.

48. Bormashenko, E.; Musin, A.; Zinigrad, M., Evaporation of droplets on strongly and weakly pinning surfaces and dynamics of the triple line. *Colloids and Surfaces A: Physicochemical and Engineering Aspects* **2011**, *385* (1-3), 235-240.

49. Weon, B. M.; Je, J. H., Self-pinning by colloids confined at a contact line. *Physical review letters* **2013**, *110* (2), 028303.

50. Watanabe, S.; Inukai, K.; Mizuta, S.; Miyahara, M. T., Mechanism for Stripe Pattern Formation on Hydrophilic Surfaces by Using Convective Self-Assembly. *Langmuir* **2009**, *25* (13), 7287-7295.

51. Colosqui, C. E.; Morris, J. F.; Stone, H. A., Hydrodynamically driven colloidal assembly in dip coating. *Physical review letters* **2013**, *110* (18), 188302.

52. Yin, T.; Shin, D.; Frechette, J.; Colosqui, C. E.; Drazer, G., Dynamic Effects on the Mobilization of a Deposited Nanoparticle by a Moving Liquid-Liquid Interface. *Physical review letters* **2018**, *121* (23), 238002.

Supporting Information

Dual-Scale Nanostructures via Evaporative Assembly

Sunita Srivastava, Zaibudeen A Wahith, Oleg Gang, Carlos E. Colosqui, Surita R. Bhatia**

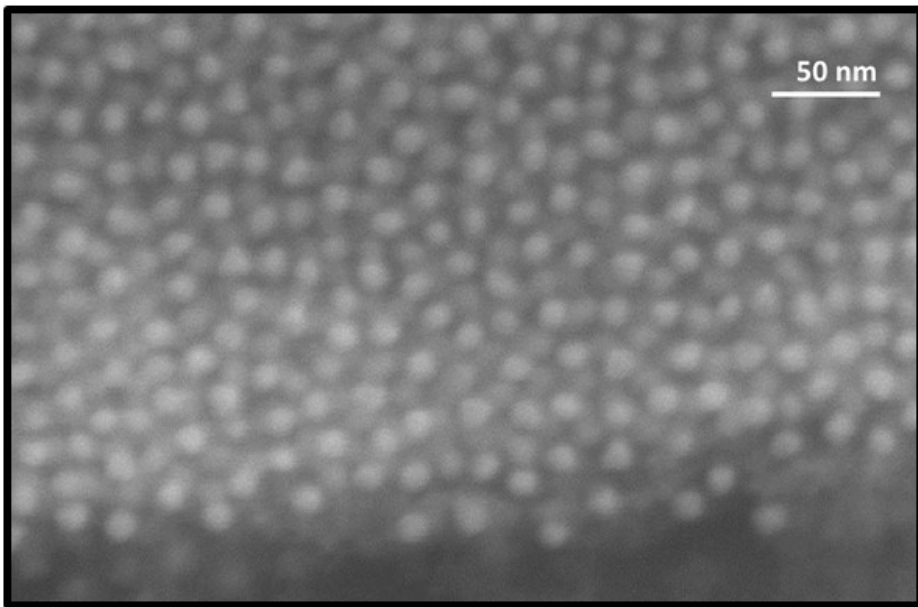


Figure S1: Outer edge of dried droplet, showing multilayer deposition of particles. By contrast, stripes in inner rings (Fig 2b, c, main text) are monolayers.

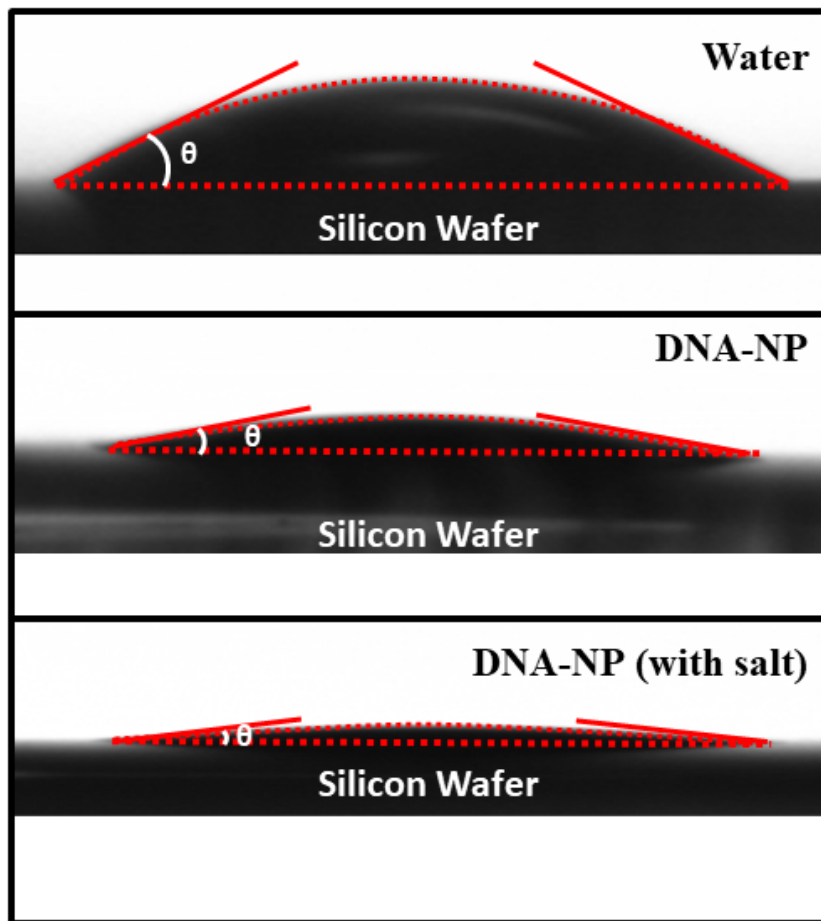


Figure S2: Images used to obtain contact angle estimates for water ($41^{\circ}\text{C} \pm 5^{\circ}\text{C}$), DNA-NP suspension ($12^{\circ}\text{C} \pm 3^{\circ}\text{C}$) and DNA-NP suspension with salt ($7^{\circ}\text{C} \pm 3^{\circ}\text{C}$), at the initial stage immediately after a drop is cast.

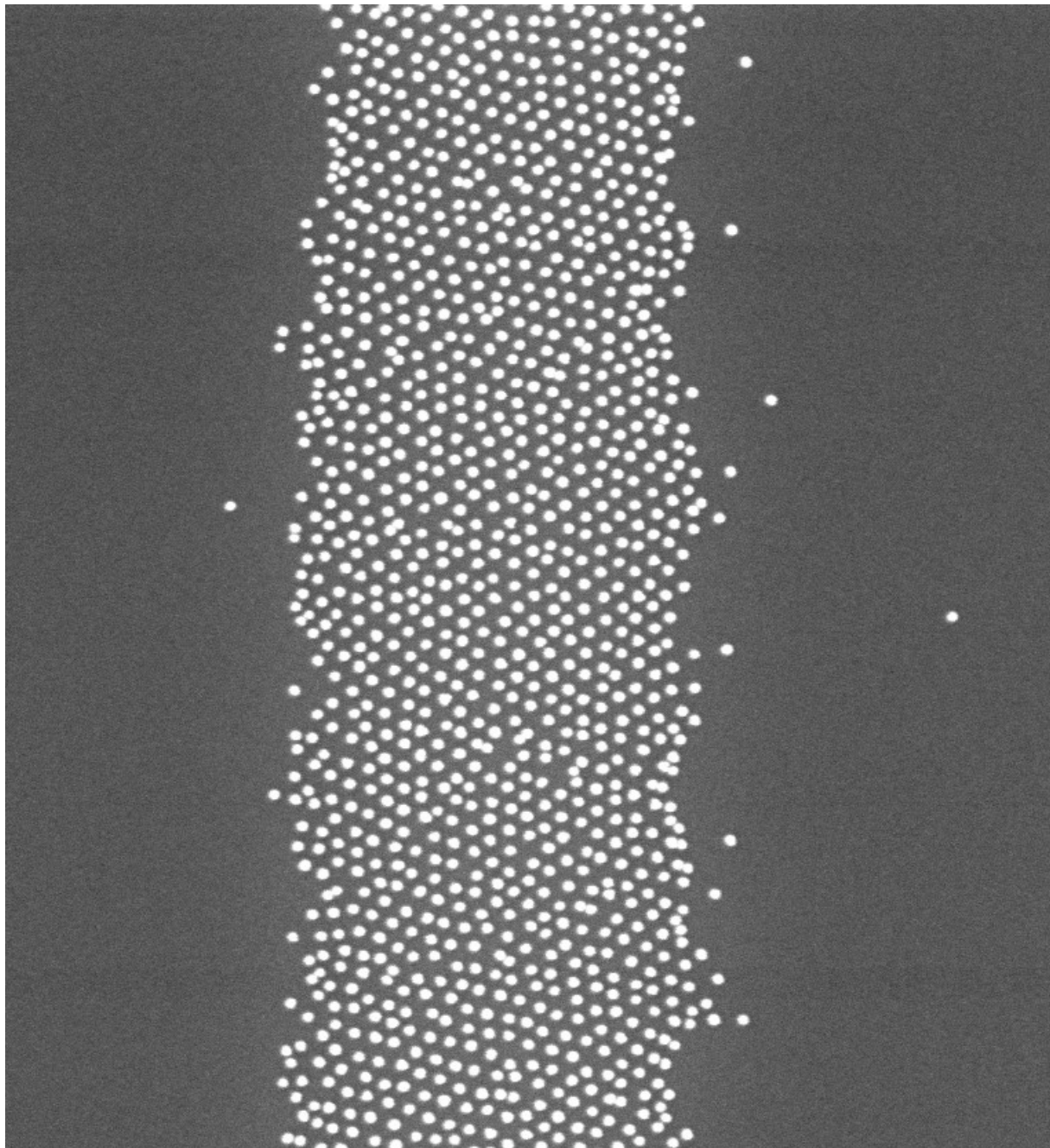


Figure S3: Increased magnification of nanoscale NP monolayer structure inside the deposited stripes at 5 nM (conditions corresponding to images in Fig. 3b, f, and j).

Table. 1 : Sequence of DNA chains used for DNA-NP functionalization

5'-/5thiolMC6-D/TTT TTT TTT TTT CGT TGG CTG GAT AGC TGT GTT CTT AAC
CTA ACC TTC AT-3'